

Electrochemistry of ethanol and dimethyl ether at Pt in a Protic ionic liquid: The electrode poisoning mechanism

Sayyar Muhammad* ^{a, b}, Darren Anthony Walsh ^a

^a School of Chemistry, *GSK Carbon Neutral Laboratory for Sustainable Chemistry*
University of Nottingham NG7 2TU, UK

^b Department of Chemistry, Islamia College Peshawar, Peshawar 25120, Pakistan

*Corresponding author

Email address: sayyar@icp.edu.pk

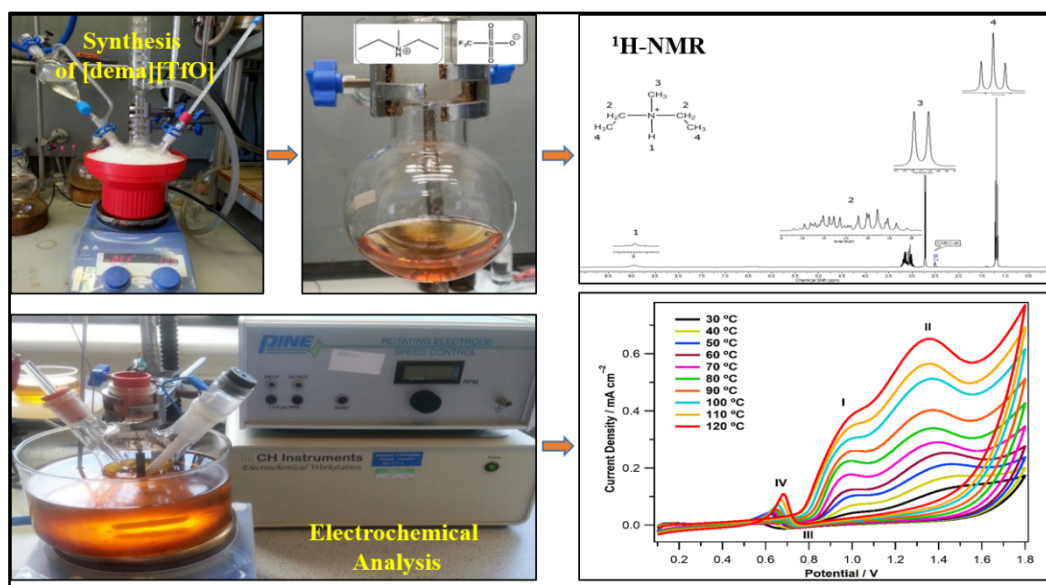
ORCID: <https://orcid.org/0000-0001-6182-9750>

Abstract

A protic ionic liquid (PIL), N, N- diethyl-N-methyl ammonium trifluoromethane sulfonate, [dema][TfO] was synthesized and confirmed through ¹H-NMR and ion chromatography (IC). The surface electrocatalysis of ethanol (EtOH), and dimethyl ether (DME) were investigated on a polycrystalline Pt electrode in the PIL using a cyclic voltammetry technique. The voltammetry response shows that the surface Pt-oxides/hydroxides (PtOH/PtO) are formed due to the oxidation of trace water (240 ppm determined by coulometric Karl-Fischer (FT) titration) in [dema][TfO] which plays a pivotal role during the electrocatalytic oxidation of EtOH and DME in the PIL. Oxidation of EtOH, and DME coincides with coverage of the Pt surface by the adsorbed oxide species that helps to activate both processes by oxidizing the adsorbed poisoning CO and CO-like intermediate species via a 'bifunctional' reaction mechanism. The influence of temperatures was investigated to obtain quantitative and qualitative information on the kinetics of EtOH oxidation. Higher activation energies are measured for EtOH oxidation in [dema][TfO] than in aqueous electrolytes due to low water content and high viscosity of the PIL. This study gave a basic insight into the mechanism of EtOH, and DME oxidation reactions, and the Pt-electrode poisoning species formation mechanism in the neoteric electrolyte medium is electrochemically investigated and reported.

Keywords: activation energy; cyclic voltammetry; dimethyl ether; electrocatalysis; ethanol oxidation; ionic liquids;

Graphical Abstract



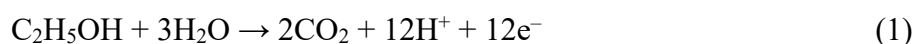
Introduction

The electrooxidation of renewable fuels, especially of small organic molecules such as methanol (MeOH), ethanol (EtOH), formaldehyde (HCHO), formic acid (FA), and dimethyl ether (DME) is important in view of their great potential in energy-conversion-relevant technologies such as direct liquid fuel cells (DLFCs) [1]. DLFCs provide carbon-neutral, sustainable, and efficient power generation prospects [2]. Direct ethanol fuel cells (DEFCs) that involve the use of EtOH as fuel, are low environmental pollution-causing electrochemical devices. Due to their increased theoretical efficiencies, they are also seen as appealing alternatives to heat engines and as one of the potential alternatives to traditional combustion technologies. However, low practical efficiencies, low power density, and the formation of acetaldehyde and acetic acid byproducts, as well as carbon monoxide, intermediates, impede the development and commercialization of DEFCs [3]. Direct dimethyl ether fuel cell (DDMEFC) that involves DME as fuel is a good choice for a portable power source. Theoretically, DDMEFCs perform better than conventional direct-feed fuel cells, but further electrochemical and operating system research is still needed. So, before DDMEFC can be commercialized, more research and advancements need to be made [4, 5].

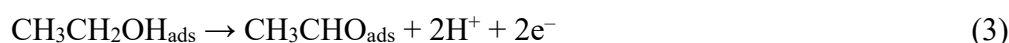
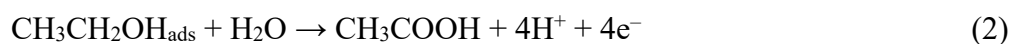
Ethanol or ethyl alcohol (C₂H₆O) is a liquid at room temperature and can be used as an excellent alternative to oil-derived fuels. Ethanol is less toxic than other alcoholic fuels (e.g., butanol), can be obtained from renewable raw materials, and has lower emissions of pollutants than fossil fuels because the oxygen that it contains improves combustion [6]. Also, ethanol is a secure, abundant, and renewable feedstock that is easily handled and stored by the existing

infrastructure. The electrochemical oxidation of ethanol has drawn increasing interest in electrocatalysis and fuel cells in recent years due to its large-scale production from biomass, low toxicity, renewability, high boiling point, and high theoretical energy density (97%) compared to other alcohols [7-12].

The oxidation of EtOH in aqueous media at Pt catalyst is a complex multiple-electron process that involves the transfer of twelve electrons and twelve protons (Eqn. 1).

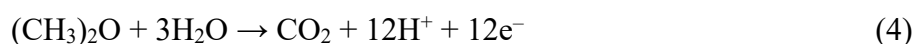


EtOH oxidation proceeds via a so-called dual-pathway mechanism. The first mechanistic pathway proceeds via CO_{ads} intermediate to form CO_2 in an acid solution (or carbonate in alkaline solutions) by delivering 12 electrons. The second pathway mainly leads to the formation of acetic acid (or acetate in alkaline solutions) by delivering four electrons (Eqn. 2) and/or acetaldehyde by delivering two electrons (Eqn. 3) [9].



The electrocatalytic oxidation of EtOH is complicated and the main challenge is the cleavage of the C–C bond, which makes complete oxidation of the EtOH difficult, resulting in a slow kinetics of the reaction in aqueous electrolytes. Pt is the most commonly used anode catalyst for EtOH oxidation due to its excellent properties in the adsorption and dissociation of ethanol. The Pt-catalyst poisoning by strongly adsorbed intermediates, e.g. CO_{ads} that results from the dissociation of EtOH at low temperatures is another electrocatalytic problem that arises due to the relative complexity of the reaction mechanisms [9-13]. Therefore, the mechanistic investigation as well as designing of an electrocatalyst that is efficient in the breaking of the C–C bond in EtOH are yet essential challenges required for the desired complete oxidation to CO_2 .

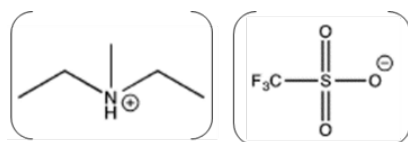
Dimethyl ether, DME ($\text{C}_2\text{H}_6\text{O}$) is a functional group isomer of EtOH, shows facile electrooxidation activity due to its unique chemical structure (two C–O bonds but no C–C bonds) compared to EtOH and oxidizes completely in the presence of H_2O to CO_2 providing 12 electrons and 12 protons (Eqn. 4) [14-16].



Pt and Pt-based electrocatalysts are mostly used for DME electrooxidation in aqueous electrolytes. However, the reaction mechanism has not been well understood compared to the oxidation of other organic fuels such as methanol and formic acid [14, 17, 18], hence; different mechanisms have been proposed for the reaction. Various surface adsorbed intermediates such as $(\text{CH}_3\text{OCH}_2^-)_{\text{ads}}$, $(\text{CH}_3\text{OC}^-)_{\text{ads}}$, $(\text{HCO})_{\text{ads}}$, and CO_{ads} along with traces of methanol and formic

acid have been detected during DME electrooxidation at Pt in acid electrolytes by Muller *et al.* [19] using cyclic voltammetry and gas chromatography studies, and Shao *et al.* [20] using surface-enhanced infrared absorption spectroscopy and cyclic voltammetry. Similar to ethanol oxidation [21], DME oxidation also requires surface oxidants (O/OH_{ads}) for the removal of surface poisoning species [14].

Protic ionic liquid (PIL) electrolytes have attracted widespread interest as promising solvents for electrochemistry due to their unique physiochemical properties, completely different from ordinary molecular liquids. PILs possess low melting points, negligible volatility and low vapor pressure at ambient temperature, intrinsic ionic conductivity, high polarity, and thermal, chemical, and electrochemical stability [22-25]. Many researchers have proposed that PILs could be used in electrochemical devices such as Li-ion batteries and fuel cells [26-28] but before such developments can be realized, it is important that we develop a thorough understanding of electrocatalysis in these unique liquids. The oxidation of trace water present in PILs can yield adsorbed oxide species (O/OH_{ads}) at a Pt surface that can affect various electrocatalytic processes [21, 26, 29, 30]. Both EtOH oxidation [29] and DME oxidation [14] can require surface oxidants (O/OH_{ads}) for the removal of surface-poisoning species. Therefore, it could be interesting to study the electrocatalysis of the oxidation of EtOH and DME and the reaction mechanism in PILs. In this regard, we synthesized N, N-diethyl-N-methyl ammonium trifluoromethane sulfonate, [dema][TfO], Scheme 1 and then investigated electrocatalytic oxidation of EtOH and DME on at Pt catalyst in it by cyclic voltammetry and describe here the catalytic effect of the surface Pt-oxides on the electrocatalysis of EtOH and DME oxidation in the liquid. The effect of temperature on the electrocatalysis of EtOH is investigated and activation energy is deduced for the process. The mechanistic investigation of the species that poison the catalyst in the neoteric PIL medium is also identified electrochemically. We have reported for the first time the mechanism and electrochemical quantification of the intermediates that poison the electrode during DME oxidation in the neoteric PIL medium which is the main novelty of this work. Also, the determination of activation energies for ethanol oxidations in the aqueous medium is reported but we determined activation energy for the EtOH oxidation in the [dema][TfO] and explained why the electrocatalysis process is slow in the IL medium. To the best of our knowledge, no such studies are undertaken for the electrooxidation of EtOH and DME in the PIL, [dema][TfO]. The experimental results presented will give an insight into understanding the mechanism of anodic oxidation of EtOH and DME at Pt in a PIL environment.



Scheme 1: Structure of [dema][TfO]

2. Materials and Methods

2.1. Reagents and Apparatus

Ethanol (absolute, 99.99 %) and dimethyl ether (DME, 99.99 %) were obtained from Fisher Chemicals and BOC gases (Nottingham, UK), respectively, and were used as received. [dema][TfO] was synthesized from the precursor Brønsted acid, trifluoromethane sulphonic acid, TFOH ($\geq 99\%$, Sigma Aldrich), and base, N, N-diethyl-N-methyl amine (95% Alfa Aesar) using the methods described elsewhere [22, 31, 32]. To describe the process briefly, equimolar amounts of the acid and base in each case were reacted together in a dry three-necked flask. Since the acid-base reactions were highly exothermic, the addition of acid to the base was carried dropwise, and the temperature was controlled and kept around $0\text{ }^{\circ}\text{C}$ using an ice bath. A slight excess of the base was used in each case to ensure complete neutralization of the acid. The mixtures were stirred continuously in an argon atmosphere during the reaction, and once the reactants were all added, stirring continued for another 2-3 hours at room temperature. The synthesized PILs were then dried under vacuum (6×10^{-2} mbar) at $70\text{ }^{\circ}\text{C}$ for 48 hours to remove excess base along with trace water, and then stored in a desiccator over silica gel.

2.2 Characterization of [dema][TfO]

The synthesis of the PIL i.e. the transfer of a proton from the acid to the base was confirmed by collecting proton nuclear magnetic resonance ($^1\text{H-NMR}$) spectra using DPX300 NMR instruments using DMSO- d_6 as the solvent. About 20-40 mg of the PIL sample was dissolved in DMSO- d_6 and NMR spectra were recorded. Chemical shifts (δ) are reported in parts per million (ppm) and the coupling constant (J) is given in Hertz (Hz).

Water is commonly found as a trace impurity in PILs which could be due to the precursor reagents used for their synthesis and absorption of moisture from the air during the course of an experiment or during storage. Therefore, it is difficult to completely remove water from the PILs even by drying them under a vacuum at high temperatures and for a long time. The water content of the PILs may affect their physicochemical and electrochemical properties [22] and therefore the magnitude of the water contents of PILs must be measured. The trace water contents of the [dema][TfO] were determined using a coulometric Karl-Fischer apparatus (Mitsubishi Moisturemeter CA-100).

Ion chromatography is a separation and quantification technique that is used for the analysis of both organic and inorganic cations and anions in an ionic solution using the principles of liquid chromatography. It involves an eluent or mobile phase that carries the ions in the sample solution which are separated by a stationary phase, usually an ion exchange resin. The detector works on the basis of conductivity, which then measures the quantity of the eluent ions as a function of retention time and gives a plot of ion abundance versus retention time. This plot is called a chromatogram. The ions with a greater affinity for the stationary phase are retained in the column for a longer time and vice versa. The position of the peak in the chromatogram corresponds to a specific ion, and the size of the peak to the concentration of that ionic species [33].

Ion chromatography measurements of the ionic liquids were performed with an ICS-3000 DC ion chromatography system, Dionex UK, equipped with a Dionex AS20 (2×250 mm) analytical column, a Dionex CG 20 guard column (2 × 50 mm), and a conductivity detector. The eluent or mobile phase was comprised of 60 % water, 25 % acetonitrile, and 15 % 0.1 M NaOH and the flow rate used was 0.25 mL min⁻¹. 5 mg of the ionic liquid sample was dissolved in 10 mL of ultrapure H₂O. A small amount of the sample (2 mL) was injected to the column for anion peak measurement. Prior to sample injection, the column was heated to 40 °C. Voltammetry measurements were performed using a computer-controlled model CHI700C potentiostat (CH Instruments, Austin, TX).

2.3 Electrochemical Measurements

Electrochemical measurements were performed in a conventional three-electrode cell (Figure 2.6) containing a Pt flag (0.5 cm × 0.4 cm × 0.1 cm) as the counter electrode. The reference electrode was Ag/AgCl/KCl (sat.) for measurements involving aqueous solutions and Pd-H for measurements involving the PIL. The Pd-H reference electrode was prepared by first annealing the Pd wire and then inserting it into a stream of H₂ for 25–30 minutes. The Pd-H reference electrode provides a stable potential defined by the hydrogen redox equilibrium at the Pd/PIL interface [34]. In the current work, the potential of the reference electrodes was compared by measuring the onset potential for H₂ oxidation/H⁺ reduction in the PILs and this was approximately 35 mV negative of the RHE reported previously by Watanabe and co-workers in PILs [35, 36]. The working electrode was a Pt/GC electrode for EtOH oxidation measurements in the PIL and was prepared by depositing Pt nanoparticles (NPs) electrochemically on a clean GC electrode from 0.1 M HCl containing 5 mM H₂[PtCl₆].6H₂O (Pt 38 %, Sigma-Aldrich) via potential step electrolysis by stepping the potential of the working electrode from 0.5 V to -0.2 V for 1000 s vs. Ag/AgCl/KCl (sat.). The electrochemical surface

area (ECSA) of the Pt-GC catalyst was estimated to be 1.23 cm². The currents in each measurement were normalized to ECSA for oxidation of EtOH. For DME oxidation in the [dema][TfO], a 2 mm diameter Pt disk was used as a working electrode, and a geometric surface area for the oxidation of DME was used for calibration of the catalytic activity of the electrodes. For EtOH oxidation measurements, the electrochemical cell was charged with approximately 5 mL of the [dema][TfO] containing 0.5 M of EtOH. For comparison, CVs were also recorded for EtOH oxidation using 0.5 M H₂SO₄ as a supporting electrolyte. Experiments for the oxidation of DME were performed in [dema][TfO] saturated with the gas for 45 minutes. Before recording each CV, the working electrode was polished by using an aqueous 0.3-micron alumina suspension (Buehler, Lake Bluff, Illinois), then rinsed, and cleaned ultrasonically in deionized water and finally dried in a stream of N₂.

3. Results and Discussion

3.1 Characterization and Structure Identification of [dema][TfO]

At room temperature, [dema][TfO] was a liquid with melting points of -13.1°C [31]. The density of the PIL, [dema][TfO] was determined by accurately weighing 1 mL of the sample PIL, and was 1.36 g cm⁻³. The average concentration of water in [dema][TfO] determined using a coulometric Karl-Fischer titration was 240 ppm.

Figure 1 shows ¹H-NMR spectra carried out in a neat sample of [dema][TfO] at ambient temperature. A peak was observed at a chemical shift, δ of about 8.95 ppm, which corresponds to the proton attached to the N of the amine after transferring from the Brønsted acid during its synthesis. This shows that the ionic liquid has been successfully synthesized. The two methylene protons (shown as 2 in the figure) appear at a chemical shift between 2.94 to 3.22 showing complex multiplicity due to coupling with the protons of the neighboring methyl groups. The behavior is reminiscent of that observed by Mori *et al.*, [37] which they attribute to the restricted rotation of the N—C bond due to steric hindrance in [dema][TfO] at ambient temperature. Also, this complex behavior of methylene group protons could be the result of coupling with the N—H proton. The methyl group protons appeared in the spectrum from 1.0 to 2.75 ppm. The peak associated with the protons of the methyl group attached directly to N (shown as 3 in the figure) was observed at 2.71 ppm as a duplet with a coupling constant 5.1 Hz and that of methyl groups (shown as 4 in the figure) attached to methylene as a triplet at 1.18 ppm with a coupling constant 7.3 Hz. The overall peak positions along with their multiplicity and coupling constants are summarized below the Figure 1 legend:

IC analysis for the [TfO]⁻ anions in [dema][TfO] was performed. The chromatogram shows a sharp peak at a retention time of 6.71 minutes (inset Figure 1). Peak retention times were compared to the anion chromatograms of silver triflate, TfOAg (CF₃SO₃Ag) which confirmed the [TfO]⁻ ions in the PILs.

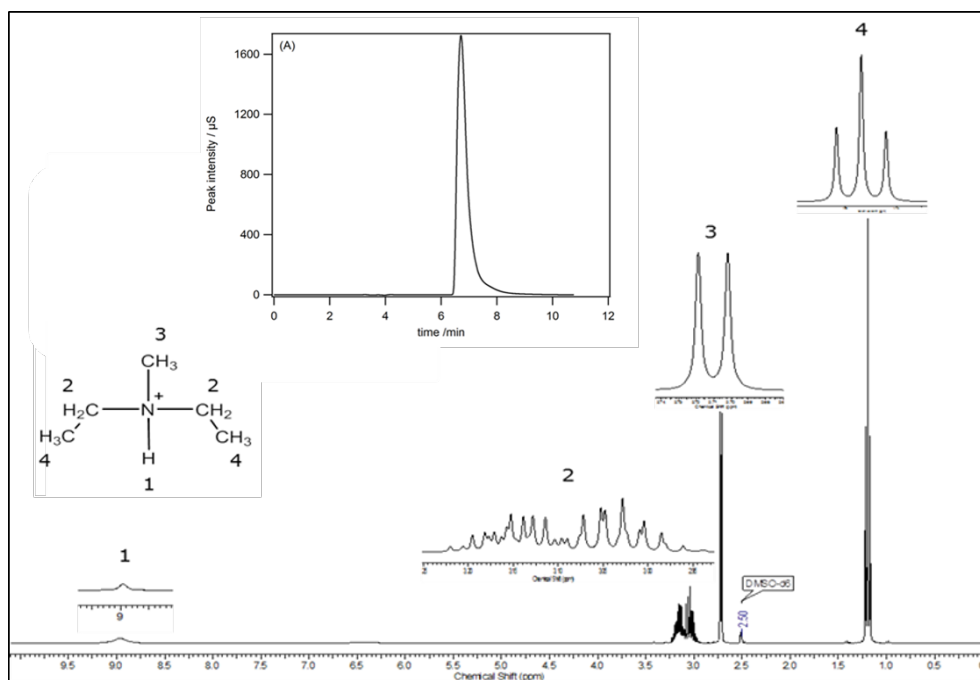


Figure 1: ¹H-NMR of [dema][TfO] in DMSO-d₆ $\delta H = 1.18$ (*t*, $J = 7.3$ Hz, 6H), 2.71 (*d*, $J = 5.1$ Hz, 3H), 2.94–3.22 (*complex multiplets*, 4H), 8.95 (*s*, 1H). The Inset of the figure shows an ion chromatogram for the anion of [dema][TfO].

3.2 Electrocatalytic oxidation of EtOH in [dema][TfO]

The electrochemical behavior of the Pt/GC catalyst during EtOH oxidation in H₂SO₄ (aq.) and in the PIL, [dema][TfO] electrolytes are shown in Figure 2. Figure 2 (a) shows the cyclic voltammograms of the Pt/GC catalyst in N₂ saturated 0.5 M EtOH in 0.5 M H₂SO₄ (aq.) and (b) 0.5 M EtOH in [dema][TfO] at 30 °C. The black dash lines in each of these figures (a) and (b) shows the blank CVs (dash line) recorded in N₂ saturated 0.5 M H₂SO₄ (aq.) and [dema][TfO] without EtOH, respectively. In the CVs (Figure 2) after the capacitive current from 0.3 V to < 0.8 V, an oxidative wave starts appearing above 0.8 V in 0.5 M H₂SO₄ (aq.) (dotted CV) and above 1.0 V in [dema][TfO] (dotted CV) corresponds to the formation of surface Pt-oxide/hydroxide (PtOH/PtO) adsorbed species which are reduced from the surface during the reverse sweep below 1.0 V in 0.5 M H₂SO₄(aq.) and below 0.8 V in [dema][TfO]. The formation of PtOH/PtO is due to the oxidation of water in the mediums at the Pt surface

during a positive going scan [22-26]. The onset potential for the oxidation of water to PtOH/PtO in 0.5 M H₂SO₄ (aq.) is lower and the peak current is higher than that in the [dema][TfO]. It is due to the presence of more water concentration and less viscous nature of the acid medium compared to that in the PIL medium which has trace water (240 ppm) and is more viscous [22, 24].

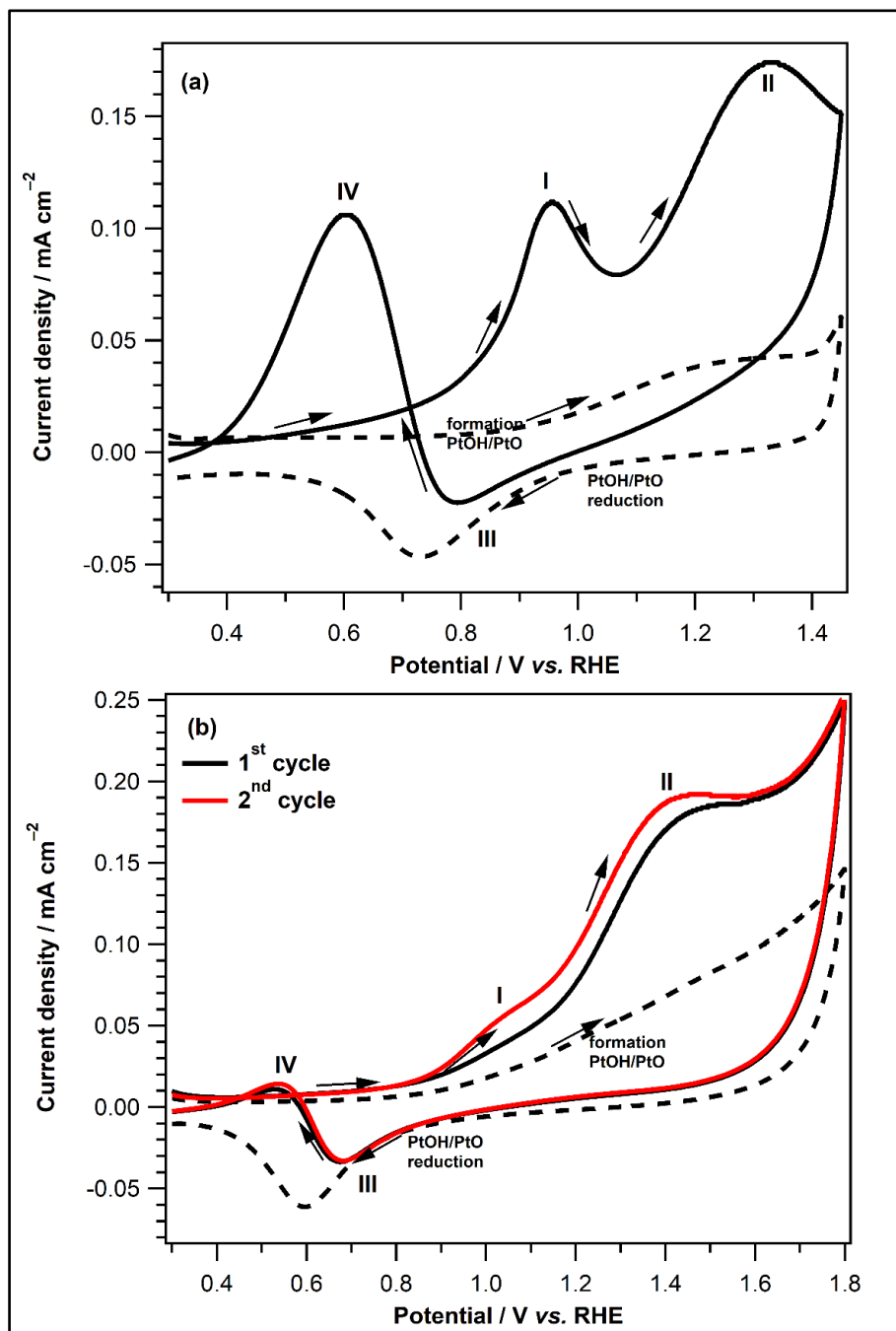


Figure 2 Cyclic voltamograms showing the oxidation of 0.5 M EtOH in (A) 0.5 M H₂SO₄ and (B) [dema][TfO] at a Pt/GC electrode at 50 mV s⁻¹ at 30 °C. The potential of the working electrode was cycled from 0.3 V to 1.45 V vs. Ag/AgCl (data reported vs. RHE) in (A) and

0.3 V to 1.8 V vs. Pd–H in (B). The dashed line in each figure shows CVs measured in each liquid saturated with N₂, before adding EtOH.

The electrochemical responses obtained for EtOH oxidation in aqueous acid is briefly described here, before discussing the electrooxidation of EtOH in [dema][TfO]. During the positive going (forward) sweep in the EtOH-containing H₂SO₄, the H_{upd} adsorption/desorption features (< 0.4 V) were inhibited compared to blank CV. The current rise for EtOH oxidation started at ~ 0.5 V and yielded two oxidation peaks, at ~0.95 V (peak I) and ~1.3 V (peak II). During the negative going (reverse) potential sweep, a small cathodic peak appeared (peak III) at 0.7 V, which corresponds to the reduction of the surface PtOH_{ads} as can be seen from the blank CV. The reduction peak is followed by an oxidation peak at a peak potential of 0.6 V (peak IV). The liberation of active Pt sites allows EtOH oxidation to recommence. These features are typical of those expected and explained for EtOH oxidation at Pt in aqueous media [38-41].

During the forward sweep, in the EtOH-containing [dema][TfO], an EtOH oxidation wave appeared at ~1.0 V that coincides with the onset of surface oxidation in blank [dema][TfO] (Figure 2 b, dashed line). This broad oxidation wave with E_p ~1.4 V (wave II) has a shoulder wave (I) that increases in magnitude in second and higher scans showing that EtOH oxidation is activated in the second and consequent scans compared to the 1st scan due to residual oxides on the electrode. The oxidation wave II also increased in magnitude and shifted to less positive potential during the second and consequent scans. On the negative sweep, similar to that in the aqueous system, the current gradually decayed and a small cathodic peak appeared (peak III) at 0.7 V that corresponds to the reduction of the PtOH_{ads} on Pt/GC catalysts in the liquid. After the regeneration of the electrode, the current due to the oxidation of EtOH again started increasing below 0.7 V and resulted in a third oxidation wave at E_p ~0.547 V (peak IV). This anodic peak appeared at the potential where PtOH_{ads} removal from the Pt surface occurred (Figure 2 b dotted line), suggesting that, during the negative sweep, EtOH oxidation restarted as some OH_{ads} were removed from the surface [29, 39].

Pt surface oxidation in [dema][TfO] starts just above 1.0 V forming PtOH_{ads} that then undergo a place exchange phenomenon at higher potentials to form PtO or PtO₂ (Figure 3) [26-28]. The two oxidation peaks, I and II obtained for EtOH electrooxidation in the ionic liquid during positive-going potential sweep can be attributed to the oxidation of the fuel by the two kinds of chemisorbed oxygen species, PtOH_{ads} and PtO, respectively. The onset of EtOH oxidation for peak I (~1.0 V) intersects with that of the onset of PtOH_{ads} formation on Pt (Figure 1 B dotted line). At higher potential (>1 V), the surface of the catalyst is further covered with

monolayers of oxide, leading to a decrease in the EtOH oxidation current. The surface oxide formed at higher potentials, mainly PtO, further facilitates EtOH oxidation by providing O species to form oxidation products. The reduction of the oxide species during the reverse sweep allows fresh adsorption and oxidation of EtOH giving peak IV. However, in the 2nd and consequent scans, some surface oxides, formed during the 1st scan, are left over on the catalyst surface that enhances EtOH oxidation leading to an increase in oxidation currents both for peak I and peak II on subsequent scans. For the electrochemical oxidation of EtOH on smooth Pt electrode in H₂SO₄, Gupta and Datta suggested a similar reaction mechanism where they associated the lower potential peak to the oxidation of ethanol and/or ethanoic residues through oxygen transfer from a PtOH_{ads} species while the second, higher potential peak from Pt–O oxygen transfer [41].

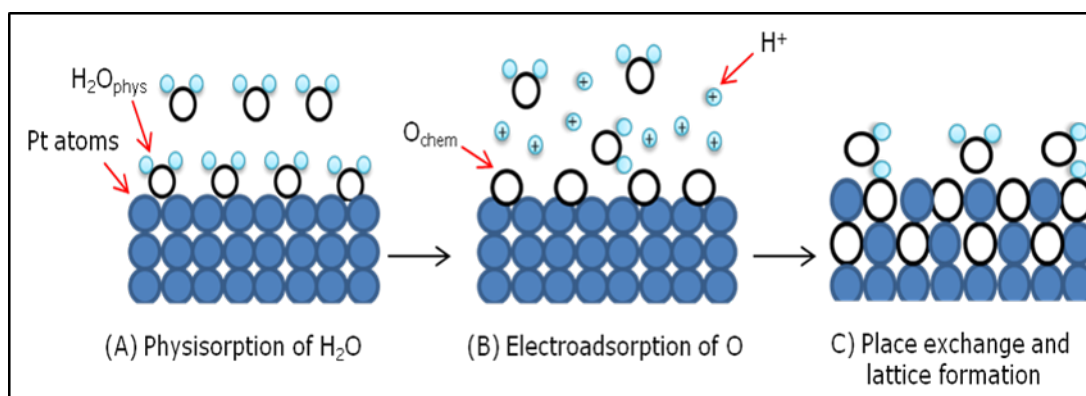


Figure 3: Mechanism of formation of Surface Pt-oxide/hydroxide species.

In the ionic liquid, the electrochemical response for EtOH oxidation is similar to that in an acid solution. The current response for EtOH oxidation in [dema][TfO] for peaks I and II is lower than for both the peaks in the acid medium. The low current response may be due to the high viscosity of [dema][TfO] and low mass transport of EtOH in the PIL compared to 0.5 M aqueous H₂SO₄. Another reason may be a lower water coverage on the Pt surface in the PIL as water is mandatory as a precursor of Pt–OH and Pt–O formation, which in turn is necessary to oxidize EtOH. However, similar to the aqueous acid solution, we also suggest that the lower oxidation peak may be due to partial oxidation of EtOH to acetaldehyde at lower potential and acetic acid at higher potential due to the provision of the O species from PtOH_{ads} and PtO formed at Pt surface from trace water in the ionic liquid at lower and higher potentials, respectively [9, 38].

3.3 Effect of Temperature on Ethanol Oxidation in the PIL

The influence of temperature on the electrocatalytic oxidation of EtOH was investigated on Pt/GC electrocatalysts in [dema][TfO]. Figure 4 (a) shows a series of CV profiles at various temperatures ranging from 30 °C to 110 °C obtained at the Pt/GC electrode in 1.0 M EtOH in [dema][TfO]. It is noted that significant activation of the electrode for the electrooxidation of EtOH was observed at elevated temperatures. With the increase in temperature of the liquid, an increase of the oxidation current with a negative shift in the onset potential during the positive going sweep and a positive shift in the re-oxidation peak during the negative going sweep was observed, as indicated by arrows in figure 4 (a). A shift of ~150 mV in the onset potential for the oxidation was observed by increasing the temperature from 30 °C to 120 °C. Also increases in the currents for peaks I, II, and IV were observed by elevating temperature from 30 °C to 120 °C. This negative shift of peak potential for EtOH oxidation is due to an increased rate of water oxidation in the PIL that leads to more surface-adsorbed OH_{ads} species [21, 24, 26, 30]. Also with increasing temperature, the onset potential of PtOH_{ads} reduction shifts positively [42], hence; a distinct positive shift of the re-oxidation peaks is observed with an increase in temperature. The increased catalytic activity of Pt/GC electrode for EtOH oxidation at elevated temperatures may also be associated with the decrease in the coverage of the electrode poisoning adsorbed intermediates such as CO_{ads} and also to the enhancement of the electrode reaction kinetics [41].

Figure 4 (b) shows Arrhenius plots of the ln (current density) versus 1/T at 1.0 V (red line) and 1.3 V (black line) for the oxidation of EtOH in [dema][TfO]. The data obtained at both of the oxidation potentials, 1.0 V and 1.3 V shows a good fit to the Arrhenius Equation, $\ln(\text{current density}) = \ln A - E_a/RT$. Where A is the pre-exponential factor or Arrhenius constant, E_a is the activation energy, R is the universal gas constant (8.3143 J K⁻¹ mol⁻¹) and T is the absolute temperature. From the plot, the activation energy calculated for EtOH oxidation in [dema][TfO] at Pt/GC electrode for the anodic peak I was 24 kJ mol⁻¹ at 1.0 V and 19 kJ mol⁻¹ at 1.3 V for the anodic peak II. The E_a value for the 1st anodic peak was higher than the 2nd anodic peak, which is supported by literature by Lee *et al.*[43],³¹ also observed a higher E_a for the anodic peak I (22.1 kJ mol⁻¹) compared to the anodic peak II (13.9 kJ mol⁻¹) for ethanol oxidation on Pt in acidic media. However, E_a is generally slightly higher in the PIL compared to aqueous systems, showing that the oxidation process is slow in the PIL. This can be seen from the low current and high onset potential for the oxidation of EtOH in [dema][TfO] compared to 0.5 M H₂SO₄ as described in Figure 2.

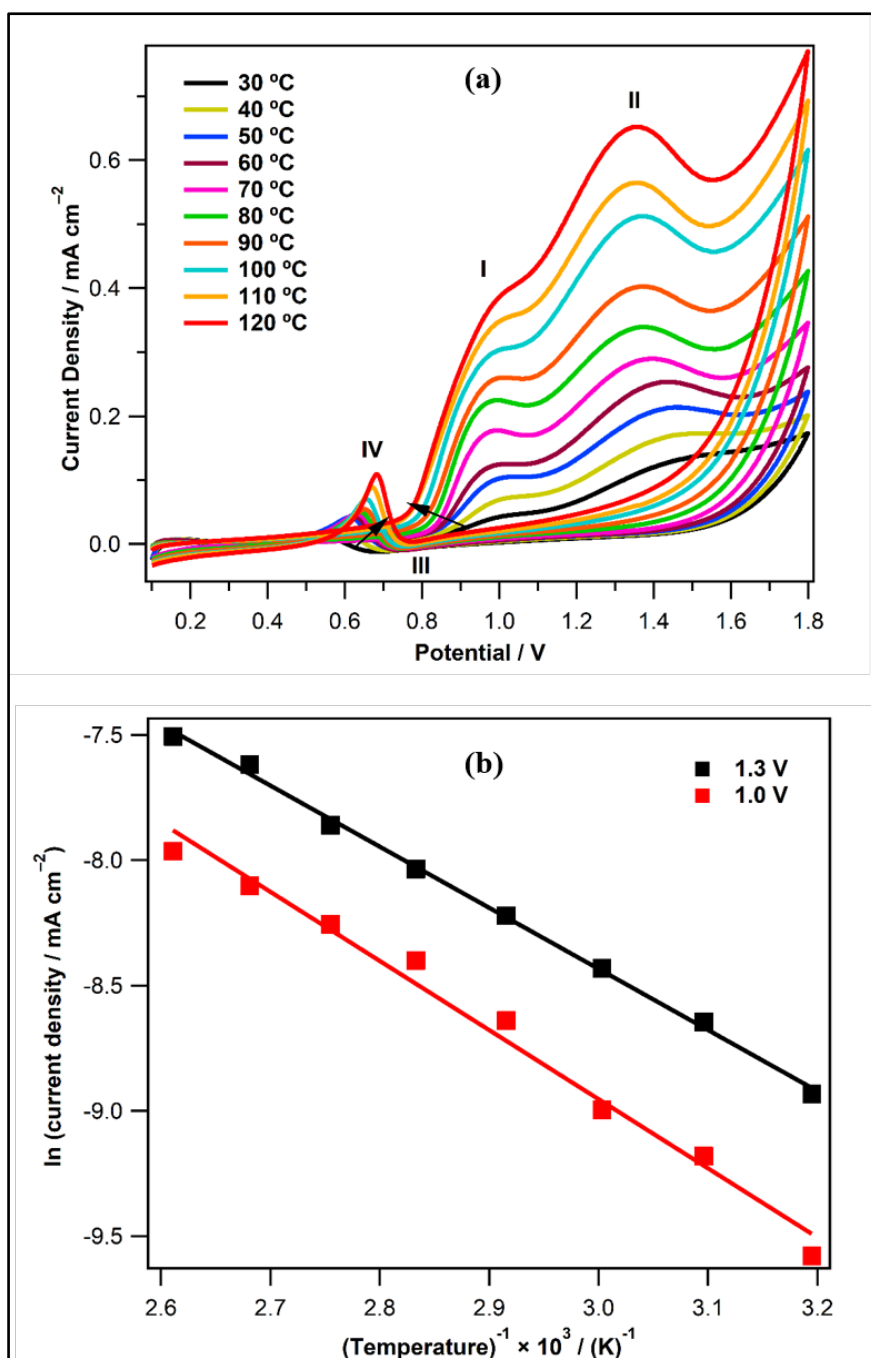


Figure 4 (a) CVs recorded on Pt/GC electrode at a series of temperatures in N₂ saturated, 1.0 M EtOH in [dema][TfO], by sweeping potential of the electrode from 0.1 V to 1.8 V at 50 mV s⁻¹. **(b)** Arrhenius plots at 1.0 V and 1.3 V for the oxidation of EtOH in [dema][TfO].

Similarly, the high activation energy obtained at a lower potential, 1.0 V vs. Pd-H in [dema][TfO] and by Lee *et al.* [43], at 0.933 V vs. RHE in acid media shows that the rate of EtOH oxidation reaction is slow at lower potentials compared to that at higher potentials, at which low activation energy was obtained. It may be due to less surface OH_{ads} species formed at lower potentials that are not sufficient to carry out complete oxidation of EtOH than at high

potential 1.3 V in [dema][TfO] where the electrode surface is covered with more oxide species. The oxide acts as a catalyst for EtOH oxidation, therefore, a lower activation energy. This continues increase in the oxidation current is obtained at 1.3 V than at 1.0 V.

3.4 Electrochemistry of dimethyl ether in the PIL

To examine the electrochemical behaviour of DME oxidation in ionic liquids, a polished 2 mm diameter Pt disk electrode was immersed in [dema][TfO] saturated with DME and CVs were recorded at 100 mV s^{-1} in a potential range between -0.05 V and 1.65 V . DME was bubbled into [dema][TfO] for 45 minutes. Figure 5 shows the voltammetry response obtained for electrooxidation of DME during the first 10 cycles at Pt in DME saturated [dema][TfO]. The dashed line in the figure shows blank CV measured in [dema][TfO] in N_2 atmosphere. Compared to the blank CV, no significant oxidation current is seen up to 0.6 V during the first positive going potential sweep (red solid line). At c.a. $\sim 0.6 \text{ V}$, an increase in current is observed and the current due to this oxidation process continued increasing until the switching potential, 1.65 V . This continuous increase in the oxidation current between 0.6 V and 1.65 V is attributed solely to DME oxidation in the liquid [15, 44, 45], catalysed by surface adsorbed Pt-oxides [14]. This result is quite similar to the results obtained by Ejigu and co-workers, during a hydrodynamic voltammetry study for methanol oxidation at Pt in the same ionic liquid [21]. However, in the second and subsequent sweeps (black solid lines) the current response due to oxidation of DME decreased until reaching a stable value in the 10th cycle (blue solid line). The onset potential for the oxidation process also shifted to the positive side in the subsequent sweeps and reaching $\sim 0.8 \text{ V}$ in the 10th sweep compared to 0.6 V in the first sweep. In the potential range between 0.6 V and 1.65 V , the 10th CV curve with DME saturated solution is not completely superimposed on the blank CV, showing that DME oxidation still happens in the 10th cycle but the current response has decreased. This decrease in current during subsequent sweeps shows that some adsorbed intermediates could be formed on the clean Pt surface during the first sweep that poisons the electrode for further oxidation in the subsequent scans leading to a decrease in the current response [15, 16, 44]. The surface oxide reduction peaks during the negative-going sweep also shifted more cathodic c.a. to 0.4 V compared to 0.7 V in the blank, due to the presence of the adsorbed intermediates formed on Pt during the positive-going sweep. However, it should be noted that the peak position for the oxides reduction wave shifted toward positive potential as the number of scans increased and was comparable to the blank in the 10th sweep where the oxide reduction was observed at 0.6 V , indicated by an arrow in the figure.

It could also be noted that the current in the H_{UPD} region (between -0.05 V and 0.40 V) is subdued significantly in the presence of DME during the first cycle compared to the current corresponding to the H-adsorption/desorption region in blank [dema][TfO]. Compared to the first cycle, the current in the H_{UPD} region increased and another oxidation wave formed in the subsequent cycles, the height of this oxidation wave at ~ 0.2 V increased and the onset potential shifted negative during subsequent scans. This oxidation wave also corresponds to the direct oxidation of DME which is catalysed by the residual surface Pt-oxides remaining on the electrode in the subsequent scans. During the first scan, the electrode surface was clean and there were no oxides present, therefore, no DME oxidation current was observed in the low potential region between -0.05 V and 0.4 V.

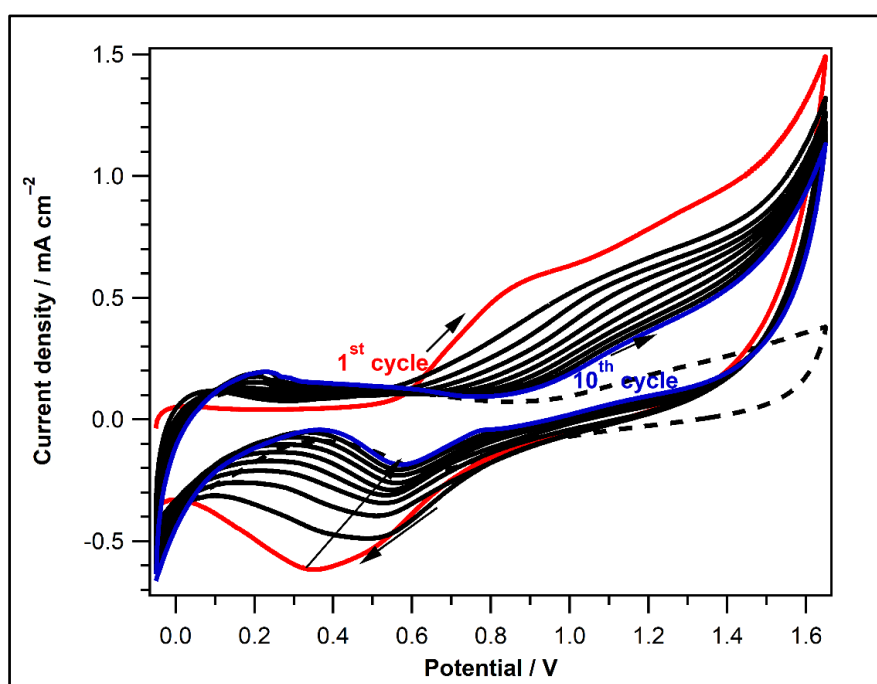


Figure 5 A series of CVs obtained for electrooxidation of DME on a 2 mm diameter Pt disk electrode at 100 mV s^{-1} in [dema][TfO] saturated with DME (solid lines) or without DME (dashed line) under N_2 atmosphere at room temperature in a potential range between -0.05 V and 1.65 V.

3.5 Electrochemical investigation of the electrode poisoning intermediates

As described above that some adsorbed intermediate species could be formed on Pt surface during first scan (red line) at potentials > 0.6 V in positive-going sweep that caused shifting of the Pt-oxides reduction wave more cathodic during the negative-going sweep (indicated by arrow in Figure 5). Zhang *et al.* [15]^{5b} has proved through an electrochemical and *in situ* IR measurements that a reaction intermediate ($-\text{CH}_2\text{OCH}_3$) can be formed in low potential region

from oxidation of DME at Pt in aqueous acid electrolyte which is then oxidized to CO_{ads} and finally to CO_2 at high potentials. In addition, Muller *et al.* [19], DME oxidation described that proceeds in many steps involving formation of reaction intermediates in lower potential region that are finally oxidized to CO_2 at higher potentials.

In order to electrochemically investigate the various potential-dependent intermediates forming during DME oxidation in [dema][TfO], we recorded CVs at freshly polished cleaned Pt by scanning the potential to 2.15 V as shown in Figure 6. A voltammetry response, similar to that in Figure 5, was obtained for the first cycle (solid black line) during positive-going sweep in which the oxidation of DME started at about 0.6 V and the current increased at high potentials and then become stable until 1.8 V after which a sharp increase in the oxidation current was observed that kept on increasing until the switching potential 2.15 V. It is worth noting that this sharp increase in oxidation current beyond 1.8 V cannot be observed in the blank CV (dashed line in the figure 6) obtained at the same electrode. This indicates that the sharp oxidation current was not due to oxidation of the anion of the ionic liquid, $[\text{TfO}]^-$ but could be due to the oxidation of the strongly adsorbed CO-like intermediates formed in the potential range between 0.6 V and 1.8 V as suggested by Zhang *et al.*[15]. The electrode seemed to be further deactivated during the second sweep (red line) and oxidation of DME above 0.6 V was suppressed compared to the first CV (black line) until 1.2 V. At around 1.2 V a sharp increase in the oxidation current was observed, which then stabilized until 1.8 V and again increased sharply in the same pattern after this potential as in the first CV (black line) but the magnitude of current was high in the second cycle. Similar voltammetry behaviour was observed in the 3rd (green line) and subsequent cycles (not shown on the figure). The sharp oxidation peak at around 1.2 V observed during 2nd and 3rd positive-going scan could be due to the oxidation CO_{ads} by $\text{Pt-OH}_{\text{ads}}/\text{PtO}_{\text{ads}}$ via Langmuir-Hinshelwood mechanism. The strongly adsorbed CO_{ads} could be formed by the oxidation of methanol which is one of the intermediate product during DME oxidation proposed by Muller *et al.*[19].

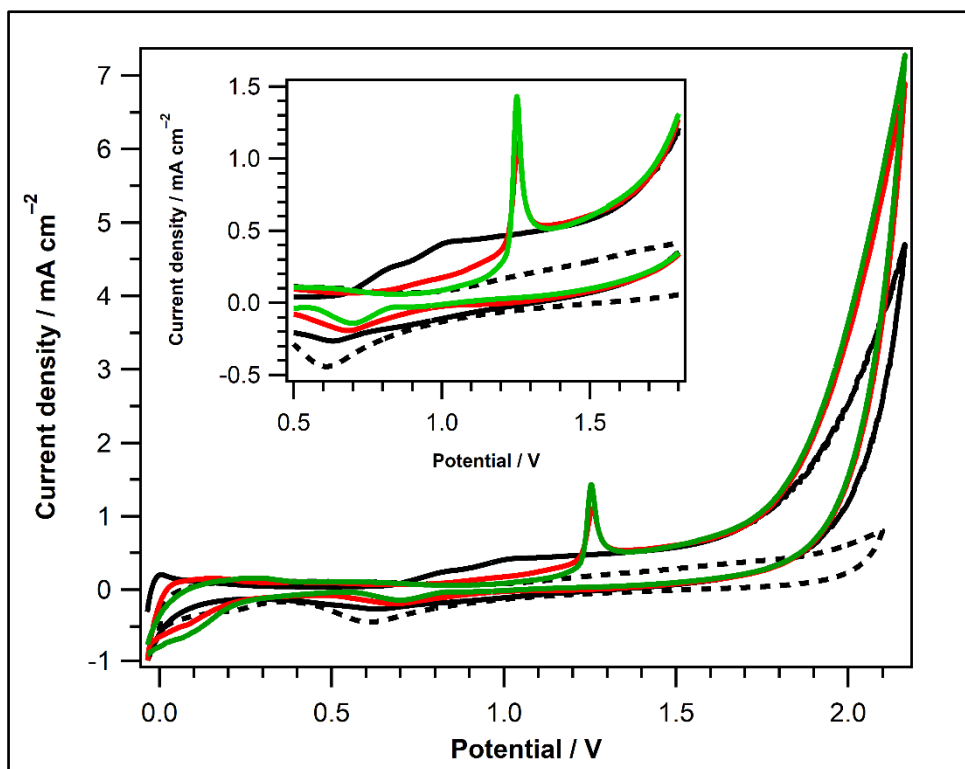


Figure 6 Three consecutive cycles (black–1st cycle, red–2nd cycle and green–3rd cycle) obtained at Pt at 100 mV s⁻¹ and 25 °C in [dema][TfO] saturated with DME in a potential range between initial potential, -0.05 V and upper potential limit, 2.15 V (inset: from 0.5 to 1.8 V) and in N₂ saturated [dema][TfO] without DME (The dashed black line).

To further investigate the surface adsorbed intermediate species forming at Pt during DME oxidation in ionic liquids, DME stripping experiment was carried out. Initially, a freshly polished clean 2 mm diameter Pt was inserted in DME saturated [dema][TfO] solution and cycled at 500 mV s⁻¹ for fifty cycles between 0.7 V and 2.3 V. The electrode was then removed from solution, rinsed with de-ionized water, dried in a stream of N₂ and CVs were obtained at 50 mV s⁻¹ in 0.2 M H₂SO₄ as shown in Figure 7. The figure shows the oxidative stripping of DME adsorbates, accumulated from DME saturated solution of [dema][TfO]. The black dash line is the blank CV obtained at a clean Pt (the same diameter) in N₂ saturated 0.2 M H₂SO₄ vs. Ag/AgCl. Compared to the blank CV, there are two main features to mention. During the first cycle (red solid line), current in the H_{upd} adsorption/desorption features (< 0.20 V) are suppressed compared to blank CV. These observations suggest that some intermediates were pre-adsorbed at Pt electrode during DME oxidation in [dema][TfO]. These adsorbates were oxidized in the broad oxidation peak that appeared at about 0.60 V, on top of the formation of surface OH_{ads} species, at Pt in the acid solution (red solid line–1st cycle). This shows that the

adsorbed species, probably $(\text{CH}_3\text{OC}^-)_{\text{ads}}$, $(\text{HCO})_{\text{ads}}$ and CO_{ads} , were electrochemically oxidized by the Pt-oxide species, OH_{ads} by Langmuir-Hinshelwood mechanism. The pre-adsorbed species were not completely stripped-off the surface in the first cycle as current in hydrogen region is still suppressed compared to blank CV and also high oxidation current is observed above 0.6 V during the second cycle (solid black line in Figure 7). In subsequent cycles oxidation current matched with that of the blank CV and the electrode was regenerated and freed of the poisonous adsorbates.

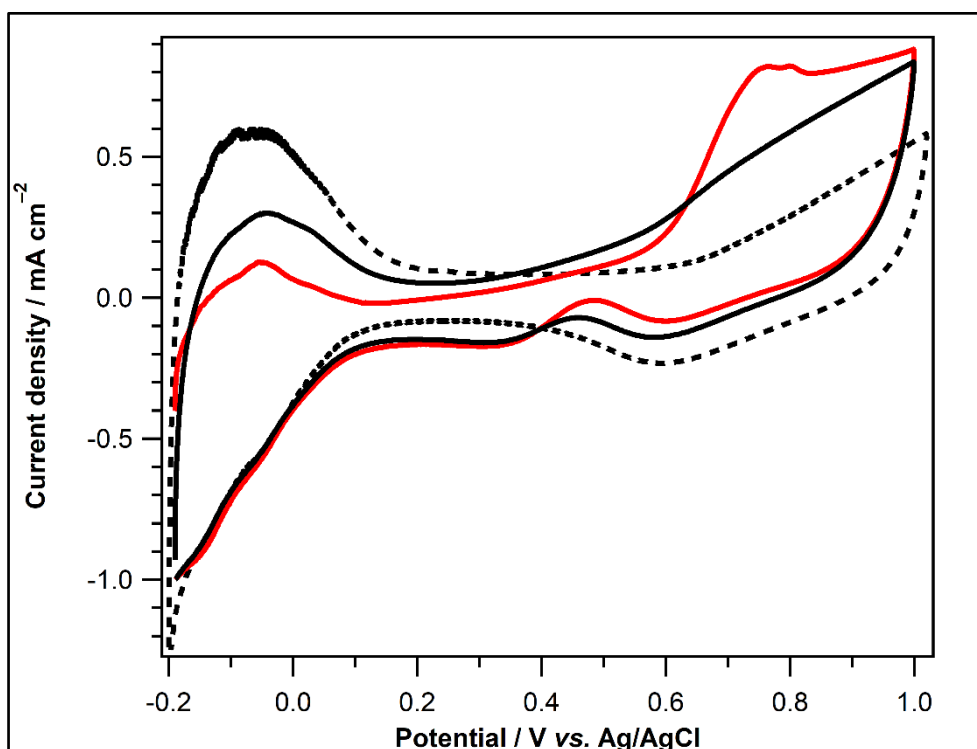


Figure 7 CVs obtained in 0.20 M H_2SO_4 (solid red line-1st cycle and black solid line-2nd cycle) showing the oxidative stripping of DME adsorbates, accumulated from DME saturated solution of [dema][TfO] after cycling the electrode at 500 mV s^{-1} in a potential range between 0.7 V and 2.3V for fifty cycles. The dashed black line is the blank CV obtained in N_2 saturated 0.2 M H_2SO_4 .

Our observations are similar to the electrooxidation of DME at Pt studied by Li and co-workers [44] in H_2SO_4 and Zhang *et al.*[15] in HClO_4 . From the oxidation of DME in [dema][TfO] at Pt catalyst, we assume that at lower potentials, intermediates such as $(\text{CH}_3\text{OCH}_2^-)_{\text{ads}}$ or $(\text{CH}_3\text{OC}^-)_{\text{ads}}$ were formed at Pt surface in the IL environment similar to aqueous systems [19, 46], which then transform at high potentials to $(\text{HCO})_{\text{ads}}$ and/or CO_{ads} and that oxidized finally to CO_2 at more positive potentials. We confirmed that the Pt-adsorbed intermediates were from

the decomposition of DME within the ionic liquid and not from the ionic liquid, through a similar chronoamperometric experiment performed in blank [dema][TfO], data not shown here.

4. Conclusion

The protic ionic liquid, [dema][TfO] was successfully synthesized as confirmed from the ¹H-NMR and IC analysis. We demonstrated that the ionic liquid [dema][TfO] could be employed as the electrolyte for electrocatalysis of ethanol and dimethyl ether at Pt electrocatalysts. It is found that the adsorbed surface oxide, OH_{ads} formed at Pt by oxidation of trace water plays an important activating role during both the oxidation processes, and helps in complete oxidation of EtOH and DME. From the cyclic voltammetric study of the electrooxidation of EtOH in [dema][TfO] at Pt/GC catalyst, we conclude that similar to EtOH oxidation in aqueous media, two oxidation peaks during positive-going potential sweep and a re-oxidation peak during reverse sweep can be obtained. However, the oxidation current density is lower for all of the three peaks compared to that in aqueous media. EtOH exhibits an increase in the oxidation current densities as temperature increases and we get high activation energies for the two-step oxidation process showing slow mass transport in [dema][TfO] due to its more viscous nature as compared to the aqueous acid medium. From the electrochemical measurement of adsorbed intermediates during DME electrocatalysis at Pt in the ionic liquid, we found that a potential-dependent chemisorption of the various intermediates occurred on Pt followed by surface processes. For facile electrocatalytic oxidation, an active electrocatalyst as well as finding, improvement and optimization of a task specific PIL is required that helps in C-C bond breaking, can promote direct oxidation of EtOH and DME, and form earlier surface adsorbed oxygen species, OH_{ads} that can help in the removal of catalyst's poisoning species such as CO_{ads}.

References

- [1] Hasan, M.M. Environment-Friendly Ascorbic Acid Fuel Cell. *Electrochem* **2023**, *4*, 31-41.
- [2] Ong, B.C.; Kamarudin, S.K.; Basri, S. Direct Liquid Fuel Cells: A Review. *Int. J. Hydrogen Energy* **2017**, *42*, 10142–10157.
- [3] Altarawneh, R. M., Overview on the Vital Step toward Addressing Platinum Catalyst Poisoning Mechanisms in Acid Media of Direct Ethanol Fuel Cells (DEFCs). *Energy & Fuels* **2021**, *35* (15), 11594-11612

- [4] Rodrigues, C. T.; de França Lopes, G.; Alonso, C. G.; de Matos Jorge, L. M.; Paraíso, P. R., An autonomous fuel cell: Methanol and dimethyl ether steam reforming direct fed to fuel cell. *International Journal of Hydrogen Energy* **2023**, *48* (10), 4052-4063;
- [5] Gebru, M. G.; Teller, H.; Subramanian, P.; Schechter, A., Nonthermal Plasma-Modified Carbon-Carrying Sn-Based Ternary Nanocatalyst for High-Performance Direct Dimethyl Ether Fuel Cells. *Energy Technology* **2022**, *10* (11), 2200835.
- [6] Susmozas, A.; Martín-Sampedro, R.; Ibarra, D.; Eugenio, M.E.; Iglesias, R.; Manzanares, P.; Moreno, A.D. Process Strategies for the Transition of 1G to Advanced Bioethanol Production. *Processes* **2020**, *8*, 1310. <https://doi.org/10.3390/pr8101310>
- [7] Wnuk, P., Jurczakowski, R & Lewera, A. Electrochemical Characterization of Low-Temperature Direct Ethanol Fuel Cells using Direct and Alternative Current Methods. *Electrocatalysis*, **2020**, *11*, 121-132.
- [8] Wang, Y.; Zou, S.; Cai, W.-B., Recent Advances on Electro-Oxidation of Ethanol on Pt- and Pd-Based Catalysts: From Reaction Mechanisms to Catalytic Materials. *Catalysts* **2015**, *5* (3), 1507-1534.
- [9] Wang, L. Q.; Bevilacqua, M.; Filippi, J.; Fornasiero, P.; Innocenti, M.; Lavacchi, A.; Marchionni, A.; Miller, H. A.; Vizza, F., Electrochemical growth of platinum nanostructures for enhanced ethanol oxidation. *Appl. Catal., B* **2015**, *165*, 185-191.
- [10] Ma, Y. J.; Du, Y. L.; Ye, W. C.; Su, B. Q.; Yang, M. X.; Wang, C. M., Electrocatalytic Oxidation of Ethanol on Platinum Electrode Decorated with Nd-Fe-Mo Hybrid-metallic Cyano-Bridged Mixing Coordination Polymer in Weak Acidic Medium. *Int. J. Electrochem. Sci.* **2012**, *7* (3), 2654-2679.
- [11] Habibi, B.; Dadashpour, E., Carbon-ceramic supported bimetallic Pt-Ni nanoparticles as an electrocatalyst for electrooxidation of methanol and ethanol in acidic media. *Int. J. Hydrogen Energy* **2013**, *38* (13), 5425-5434.
- [12] Jiang, L.; Hsu, A.; Chu, D.; Chen, R., Ethanol electro-oxidation on Pt/C and PtSn/C catalysts in alkaline and acid solutions. *Int. J. Hydrogen Energy* **2010**, *35* (1), 365-372;
- [13] Demirci, U. B., Theoretical means for searching bimetallic alloys as anode electrocatalysts for direct liquid-feed fuel cells. *J. Power Sources* **2007**, *173* (1), 11-18
- [14] Li, Q.; Wu, G.; Johnston, C. M.; Zelenay, P., Direct Dimethyl Ether Fuel Cell with Much Improved Performance. *Electrocatal.* **2014**, *5* (3), 310-317.
- [15] Zhang, Y.; Lu, L. L.; Tong, Y. J.; Osawa, M.; Ye, S., Electrochemical and infrared study of electro-oxidation of dimethyl ether (DME) on platinum polycrystalline electrode in acid solutions. *Electrochim. Acta* **2008**, *53* (21), 6093-6103;

- [16] Lu, L. L.; Yin, G. P.; Tong, Y. J.; Zhang, Y.; Gao, Y. Z.; Osawa, M.; Ye, S., Electrochemical behaviors of dimethyl ether on platinum single crystal electrodes. Part I: Pt(111). *J. Electroanal. Chem.* **2008**, *619*, 143-151.
- [17] Herron, J. A.; Ferrin, P.; Mavrikakis, M., First-Principles Mechanistic Analysis of Dimethyl Ether Electro-Oxidation on Monometallic Single-Crystal Surfaces. *J. Phys. Chem. C* **2014**, *118* (42), 24199-24211.
- [18] Si, F.; Liao, J.; Liang, L.; Liu, C.; Zhang, X.; Xing, W., Investigation of Pt nanoparticles with controlled size supported on carbon for dimethyl ether electrooxidation. *J. Power Sources* **2013**, *225*, 231-239.
- [19] Muller, J. T.; Urban, P. M.; Holderich, W. F.; Colbow, K. M.; Zhang, J.; Wilkinson, D. P., Electro-oxidation of dimethyl ether in a polymer-electrolyte-membrane fuel cell. *J. Electrochem. Soc.* **2000**, *147* (11), 4058-4060.
- [20] Shao, M. H.; Warren, J.; Marinkovic, N. S.; Faguy, P. W.; Adzic, R. R., In situ ATR-SEIRAS study of electro oxidation of dimethyl ether on a Pt electrode in acid solutions. *Electrochem. Commun.* **2005**, *7* (5), 459-465.
- [21] Ejigu, A.; Johnson, L.; Licence, P.; Walsh, D. A., Electrocatalytic oxidation of methanol and carbon monoxide at platinum in protic ionic liquids. *Electrochem. Commun.* **2012**, *23*, 122-124.
- [22] Muhammad, S., Zahra, U. B., Hajra, W., Daud, A., Sannan, M., Waqas, M., Saiqa, S., Bushra, N., Kamran, K., Shabir A. Assessment of the Hygroscopic Behaviour of Proton-Conducting Ionic Liquids: Kinetics, Conductivity and Electrochemical Analysis, *Journal of the Electrochemical Society.* **2023**, *170* (4), 046506.
- [23] Jalal, K., Muhammad, S., Luqman, A. S., Javed, A., Ibrar, M., Khushnood, U. R. Synthesis, characterization and electrochemistry of triethyl ammonium sulphate ionic liquid, *Z. Phys. Chemie.*, **2021**, *235*(9): 1099–1111.
- [24] Muhammad, S., Jalal, K., Sadia, J., Riffa, I., Hajra, W., Luqman, A. S., Kamran, K., Shabir, A., Synthesis and Physioelectrochemical Characterization of Triethylammonium bisulphate Ionic Liquid and the Role of the Electrode Surface Oxides during Ethanol Oxidation, *Chem. Phys. Lett.*, **2020**, *758*, 137902.
- [25] Goodwin, S., Muhammad, S., Li-Ping T. Walsh, D. The Contrasting Role of Parent Amines during Reduction of Proton and Oxidation of Protic Ionic Liquids. *J. Electroanal. Chem.* **2018**, *819*, 187–192.

- [26] Walsh, D. A.; Ejigu, A.; Muhammad, S.; Licence, P., The Formation and Role of Oxide Layers on Pt during Hydrazine Oxidation in Protic Ionic Liquids. *Chemelectrochem* **2014**, *1* (1), 281-288.
- [27] MacFarlane, D. R.; Tachikawa, N.; Forsyth, M.; Pringle, J. M.; Howlett, P. C.; Elliott, G. D.; Davis, J. H.; Watanabe, M.; Simon, P.; Angell, C. A., Energy applications of ionic liquids. *Energy Environ. Sci.* **2014**, *7* (1), 232-250
- [28] Menne, S.; Pires, J.; Anouti, M.; Balducci, A., Protic ionic liquids as electrolytes for lithium-ion batteries. *Electrochem. Commun.* **2013**, *31*, 39-41.
- [29] Ejigu, A.; Johnson, L.; Licence, P.; Walsh, D. A., Electrocatalytic oxidation of methanol and carbon monoxide at platinum in protic ionic liquids. *Electrochem. Commun.* **2012**, *23*, 122-124.
- [30] Walsh, D. A.; Ejigu, A.; Smith, J.; Licence, P., Kinetics and mechanism of oxygen reduction in a protic ionic liquid. *Phys. Chem. Chem. Phys.* **2013**, *15* (20), 7548-7554.
- [31] Nakamoto, H.; Watanabe, M., Brønsted acid-base ionic liquids for fuel cell electrolytes. *Chem. Commun.* **2007**, (24), 2539-2541.
- [32] Belieres, J. P.; Angell, C. A., Protic ionic liquids: Preparation, characterization, and proton free energy level representation. *J. Phys. Chem. B* **2007**, *111* (18), 4926-4937.
- [33] Weiss, J. *Handbook of Ion Chromatography, 3 Volume Set*. Vol. 1. John Wiley & Sons, 2016.
- [34] Bautista-Martinez, J. A.; Tang, L.; Belieres, J. P.; Zeller, R.; Angell, C. A.; Friesen, C., Hydrogen Redox in Protic Ionic Liquids and a Direct Measurement of Proton Thermodynamics. *J. Phys. Chem. C* **2009**, *113* (28), 12586-12593.
- [35] Yasuda, T.; Nakamura, S.; Lee, S. Y.; Watanabe, M., Performance of Nonhumidified Intermediate-temperature Fuel Cells Based on Protic Ionic Liquids Prepared from Oxo and Amide Acids. *Chem. Lett.* **2010**, *39* (7), 678-679.
- [36] Lee, S. Y.; Ogawa, A.; Kanno, M.; Nakamoto, H.; Yasuda, T.; Watanabe, M., Nonhumidified Intermediate Temperature Fuel Cells Using Protic Ionic Liquids. *J. Am. Chem. Soc.* **2010**, *132* (28), 9764-9773.
- [37] K. Mori, S. Hashimoto, T. Yuzuri and K. Sakakibara, *Bull. Chem. Soc. Jpn.*, **2010**, *83*, 328-334.
- [38] Habibi, B.; Dadashpour, E., Carbon-ceramic supported bimetallic Pt-Ni nanoparticles as an electrocatalyst for electrooxidation of methanol and ethanol in acidic media. *Int. J. Hydrogen Energy* **2013**, *38* (13), 5425-5434;

- [39] Sieben, J.; Duarte, M., Nanostructured Pt and Pt–Sn catalysts supported on oxidized carbon nanotubes for ethanol and ethylene glycol electro-oxidation. *Int. J. Hydrogen Energy* **2011**, *36* (5), 3313-3321;
- [40] Puthiyapura, V.; Brett, D.; Russell, A.; Lin, W.; Hardacre, C., Development of a PtSn bimetallic catalyst for direct fuel cells using bio-butanol fuel. *Chem. Commun.* **2015**, *51* (69), 13412-13415;
- [41] Gupta, S. S.; Datta, J., A comparative study on ethanol oxidation behavior at Pt and PtRh electrode deposits. *J. Electroanal. Chem.* **2006**, *594* (1), 65-72.
- [42] Johnson, L.; Ejigu, A.; Licence, P.; Walsh, D. A., Hydrogen Oxidation and Oxygen Reduction at Platinum in Protic Ionic Liquids. *J. Phys. Chem. C* **2012**, *116* (34), 18048-18056.
- [43] Lee, C.-G.; Umeda, M.; Uchida, I., Cyclic voltammetric analysis of C₁–C₄ alcohol electrooxidations with Pt/C and Pt–Ru/C microporous electrodes. *J. Power Sources* **2006**, *160* (1), 78-89.
- [44] Li, Q.; Wu, G.; Johnston, C. M.; Zelenay, P., Anode Catalysts for the Direct Dimethyl Ether Fuel Cell. *ECS Trans.* **2011**, *41* (1), 1969-1977;
- [45] Kéranguéven, G.; Coutanceau, C.; Sibert, E.; Hahn, F.; Léger, J.-M.; Lamy, C., Mechanism of di (methyl) ether (DME) electrooxidation at platinum electrodes in acid medium. *J. Appl. Electrochem.* **2006**, *36* (4), 441-448.
- [46] Lu, L. L.; Yin, G. P.; Tong, Y. J.; Zhang, Y.; Gao, Y. Z.; Osawa, M.; Ye, S., Electrochemical behaviors of dimethyl ether on platinum single crystal electrodes. Part II: Pt(100). *J. Electroanal. Chem.* **2010**, *642* (1), 82-91.